ELSEVIER

Chemical Engineering Journal 119 (2006) 27–36

Chemical Engineering Journal

www.elsevier.com/locate/cej

Hydrodynamic and transport parameter sensitivity in the simulation of non-isothermal agitated gas–liquid reactors

A.A. Shaikh *, A. Jamal [1]

Department of Chemical Engineering, King Fahd University of Petroleum & Minerals, P.O. Box 5050, Dhahran 31261, Saudi Arabia

Received 12 April 2005; received in revised form 7 March 2006; accepted 9 March 2006

Abstract

A generalized mathematical model has been developed to analyze steady-state behavior of non-isothermal mechanically agitated gas–liquid reactors. The model takes into consideration gas absorption with interphase mass transfer-reaction effects on the basis of bubble sphericity; mode of physical contact; variation of transport, hydrodynamic, and associated parameters by way of empirical correlations; and reactor and impeller geometry. A numerical sensitivity study is presented for a standard-configuration reactor in which an exothermic general bimolecular, second-order, reaction takes place. The analysis demonstrates that the confluence of mode of physical contact, variation of transport, hydrodynamic, and associated parameters, can lead to remarkably different portraits of steady-state multiplicity as opposed to those reported in the literature. Important results include the signal effect of the degree of agitation on the regions and patterns of multiplicity, as well as the conservative character of the multiplicity criteria reported in earlier studies of this reactor.

Keywords: Agitated reactors; Gas–liquid reaction; Steady-state multiplicity

1. Introduction

Mechanically agitated gas–liquid reactors are commonly used in the chemical, biochemical and fine-chemicals industries. The non-isothermal behavior and particularly the existence of steady-state multiplicity in this two-phase reactor were investigated in several studies in the wake of the experimental study of Ding et al. [1]. Most of these studies [2–13] addressed, analytically or numerically, different aspects of the occurrence of multiplicity using fast or general, linear and non-linear kinetics. Other studies addressed transients associated with non-isothermal operation of agitated gas–liquid reactors, e.g. [14]. These previous works have led to rigorous modeling of non-isothermal agitated gas–liquid reactors and better understanding of their steady-state and dynamic behavior. Yet, some fundamental issues have not been addressed and thus are still open to question.

Numerous studies in the literature have shown that the performance of agitated gas–liquid reactors is not only dependent on intrinsic reaction kinetics and interphase mass transfer but, as importantly, on physical contacting as well as vessel and impeller geometry; see e.g. [15,16]. Physical contacting includes factors such as degree of agitation and consequent energy dissipation, and gas hold-up; whereas geometrical factors include elements such as vessel length/diameter ratio, impeller type, mode of gas input, and number and disposition of baffles. Although there exists a tremendous amount of research (see e.g. [17–19]) demonstrating that transport and hydrodynamic parameters are intricately wedded to physical contacting and vessel-impeller geometry, no attempt has apparently been undertaken to explicitly integrate these elements in the mathematical modeling of non-isothermal agitated reactors, nor as a consequence, in the analysis of steady-state multiplicity in this widely used contactor.

The first objective of the present investigation is to develop a generalized model to describe the performance of non-isothermal, non-adiabatic, gas–liquid mechanically agitated reactor. The model is generalized in the sense that for the first time it simultaneously takes into consideration: (a) gas absorption with general reaction kinetics that are not limited to a particular regime; (b) mode of physical contact and consequent variation in transport and hydrodynamic parameters; (c) reactor and impeller geometry. The second objective is to numerically simulate the behavior of this reactor using a common exothermic reaction in order to investigate multiplicity phenomena versus idealized models presented earlier in the literature.

* Corresponding author. Tel.: +966 3 860 2205; fax: +966 3 860 4234.
E-mail address: aashaikh@kfupm.edu.sa (A.A. Shaikh).
[1] Present address: Gas Technology Institute, Des Plaines, IL 60018, USA.

1385-8947/$ – see front matter © 2006 Elsevier B.V. All rights reserved.
doi:10.1016/j.cej.2006.03.006

Nomenclature

a	dimensionless concentration of gas reactant in liquid phase
$\underline{a}$	interfacial area per unit reactor volume
A	concentration of gas reactant in liquid phase
B	concentration of liquid reactant in liquid phase
B'	dimensionless parameter in reactor model equations, $(-\Delta H_S - \Delta H_R)A_{Gf}/\rho_L c_{pL} T_{Lf}$
c_p	specific heat
d_b	bubble diameter
D_j	diffusion coefficient of reactant j
E_A^*	reaction (or enhancement) factor
F	volumetric flow rate
H_{ag}	heat due to mechanical agitation and aeration (sparging)
H_A	Henry's law constant
H_o	dimensionless parameter, RT_{Gf}/H_A
H_p	dimensionless parameter in reactor model equations, $H_{ag}/\rho_L c_{pL} F_{Gf} T_{Lf}$
ΔH_R	heat of reaction, negative if heat is liberated
ΔH_S	heat of dissolution, negative if heat is liberated
ΔH_V	heat of vaporization, negative
k	reaction rate constant
k_G	gas-side mass transfer coefficient
k_L	liquid-side mass transfer coefficient
M	Hatta number, $(kD_A B_L)^{1/2}/k_L$
N	impeller speed
N_A	rate of gas absorption
N_G	molar gas flow rate
p	partial pressure
p'	dimensionless parameter in reactor model equations, $(-\Delta H_R)F_{Lf}A_{Gf}/\rho_L c_{pL} F_{Gf} T_{Lf}$
P	total reactor pressure
P_T	total power input
q	dimensionless parameter in reactor model equations, B_{Lf}/A_{Gf}
Q	dimensionless parameter in reactor model equations, F_{Gf}/F_{Lf}
r	dimensionless parameter in reactor model equations, $\rho_{Gf} c_{pG}/\rho_{Lf} c_{pL}$
R_A	reaction rate of species A
S	reactor cooling area
T	reactor temperature
U	overall heat transfer coefficient
v	stoichiometric coefficient
V_r	reactor volume
x	conversion
y	mole fraction in the gas phase
y_B^*	dimensionless parameter in reactor model equations, $y_{Bo}/(1 - y_{Bo})$

Greek symbols

α	dimensionless parameter in reactor model equations, $(1/Q) + r$
α'	dimensionless parameter in reaction factor, $\varepsilon_L k_L/\underline{a} D_A$
β	dimensionless parameter in reactor model equations, $US/F_{Gf}\rho_{Lf} c_{pL}$
β'	dimensionless parameter in reaction factor, $F_L/\underline{a} k_L$
γ	dimensionless parameter in reaction factor, $D_B/v D_A$
δ	dimensionless parameter in reactor model equations, $(-\Delta H_S)/RT_{Lf}$
θ	dimensionless reactor temperature, $(T - T_{Lf})/T_{Lf}$
θ_r	dimensionless ratio, T_{Gf}/T_{Lf}
λ	thermal conductivity
ν	dimensionless parameter in reactor model equations, $(-\Delta H_V)\rho_{Gf}/\rho_{Lf} c_{pL} T_{Lf}$
ρ	density
τ	residence time
ψ	dimensionless parameter in reactor model equations, $k_L/k_G H_A$
Ω	dimensionless parameter in reaction factor, $[k_L(d_b/2)/D_A] - 1$

Subscripts

c	coolant
f	feed
G	gas phase
i	gas–liquid interface
L	liquid phase
o	outlet

2. Physical contacting and reactor-impeller geometry

The mathematical modeling of gas–liquid agitated reactors is generally based on the development of material balances for reacting and inert species, energy balance for the reactor, and account of interphase reaction-transport effects. All of these however should be complimented with correlations and data for transport and hydrodynamic parameters in order to develop a truly general model. The latter include: interfacial area, gas hold-up, mass transfer coefficients in the gas and liquid sides, and heat transfer coefficients in the tank and jacket or coil sides. As we alluded to earlier, the literature shows that these basic parameters are dependent (often in a complex manner) on factors such as impeller speed, power input due to agitation and aeration (i.e. sparging), and bubble diameter. These factors in turn depend on impeller type, vessel configuration, and mechanism of gas dispersion.

A wide variety of impellers are used in practice such as the propeller, flat-blade disc turbine, and helical-ribbon type. Detailed discussions on various types of impellers can be found in many references on mixing; see e.g. [20,21]. One of the most widely used impellers for gas–liquid systems is the flat-blade disc turbine, commonly called the Rushton turbine. Most of the published experimental studies on hydrodynamics and heat- and mass-transfer characteristics in agitated reactors have been per-

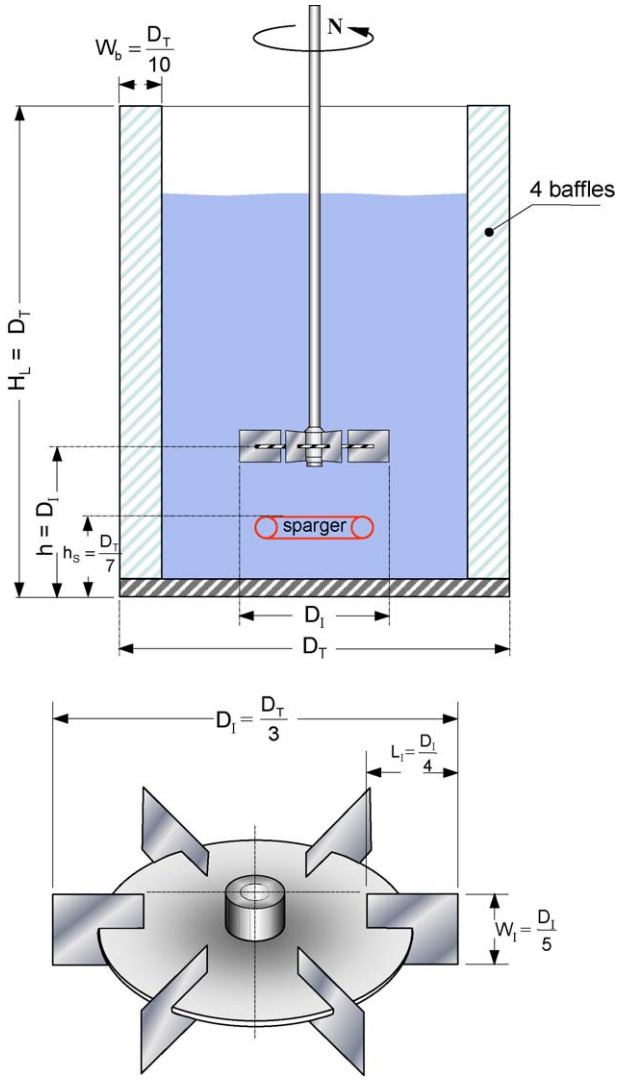

Fig. 1. Schematic diagram of a standard-configuration mechanically-agitated reactor.

formed using the standard reactor and impeller configurations. A schematic diagram of a standard reactor is shown in Fig. 1. The standard configuration is comprised of a cylindrical tank with a flat bottom, liquid and gas feed and withdrawal arrangements, Rushton turbine and a cooling/heating arrangement, which could be either a surrounding jacket or a helical coil inserted inside the tank. The gas is generally introduced at the bottom of the reactor through a ring sparger placed just below the agitator. The geometrical relationships in the standard configuration are also given in Fig. 1. The standard configuration has been widely used in research and often adopted in practice, although variations with regard to the aspect ratio (H_L/D_T) and type of impeller exist in industry [22]. Therefore, in order to gain realistic insight into the steady state behavior of agitated reactors, and to be able to assess the results of different researchers, use will be made of the standard geometry in the present analysis.

Adequate gas dispersion is essential for creating sufficient interfacial area and gas hold-up. Many authors have explained the phenomenon of gas dispersion in agitated tank reactors; see e.g. [23,24]. Niewnow et al. [25] observe that if the impeller speed is increased at a constant gas feed rate, several dispersion regimes are possible. At very low impeller speeds, the gas is not dispersed but passes around the turbine and flows along the impeller shaft forming a partial bubble column (a regime called "flooding"). By increasing the impeller speed bubbles begin to disperse in the region above the impeller forming a full bubble column. A further increase in impeller speed initiates circulation of gas below the impeller until a condition of complete dispersion is reached. At this point the gas is just thoroughly dispersed and further increase in the gas flow rate will not be useful since any additional gas will bypass the impeller shaft without being dispersed. Therefore, from the operational point of view, the complete dispersion regime is most desirable and the flooding regime is most undesirable and should always be avoided by operating the reactor at an impeller speed such that complete dispersion is achieved. It follows then that the complete gas dispersion regime can only be obtained if the reactor is operated beyond a minimum impeller speed (N_m). The impeller power consumption also is considerably reduced in case of complete gas dispersion. Therefore, for analysis and design of agitated reactors, prediction of these two quantities is essential since they have significant influence on hydrodynamic parameters. Many correlations for predicting the minimum impeller speed and power requirement in presence of gas (the so-called aerated state) have been proposed in the literature; see e.g. [26,27].

3. Reactor model formulation

A generalized model for a steady-state, non-adiabatic, gas-liquid stirred reactor will be presented below. The model considers general second-order kinetics (in the sense that the absorption-reaction regime is not fixed a priori) for the generic gas–liquid reaction: $A_{(G)} + \upsilon B_{(L)} \rightarrow$ Products. The reactor model has been developed by relaxing most of the assumptions of previous investigations. In contrast to all the previous investigations cited in Section 1, the effect of changing reactor operating conditions is incorporated in the present analysis by using empirical correlations and data for various transport, hydrodynamic, and related parameters. Furthermore, the reaction (or enhancement) factor will be used to account for the effect of reaction on interphase mass transfer. The model development is based on the following assumptions: (1) heats of solution, reaction, and evaporation are independent of temperature and conversion; (2) the feed gas is composed of reactant A and insoluble inert species; (3) the total pressure of the reactor is constant and so is the liquid volumetric flow rate; (4) the interfacial heat transfer resistance is negligible such that the gas and liquid phases are at the same temperature inside the reactor; and (5) phase equilibria of the gaseous and liquid reactants follow Henry's and Raoult's laws, respectively.

3.1. Steady-state reactor model equations

The development of reactor material and energy balances has been discussed in earlier studies; see e.g. [9,13]. Therefore only integration of new elements in the reactor model is explicated below.

Table 1
Correlations for transport, hydrodynamic, and allied parameters

Parameters	Correlation(s)
Liquid-side mass transfer coefficient (k_L)	Prasher–Wills [31]
Gas-side mass transfer coefficient (k_G)	Sharma–Mashelkar [32]
Tank-side heat transfer coefficient (h_T)	Kurpier et al. [33], Rao–Murthy [34]
Jacket-side (h_j) and coil-side heat transfer coefficient (h_c)	Lehrer [35], Bondy–Lippa [36]
Interfacial area (a), gas hold-up (ε_G), and mean bubble diameter (d_b)	Miller [37]
Bubble terminal rise velocity (u_{br})	Abu El-Hassan [38]
Minimum impeller speed (N_m)	Niewnow [27]
Power input due to agitation (P_{ag})	Warmoeskerken–Smith [39], Calderbank–Moo-Young [40]
Power input due to aeration (P_g)	Miller [37]
Total power input (P_T)	Miller [37]

- Material balances of gaseous reactant and inerts

$$N_{Gf}y_{Af} - N_{Go}y_{Ao} = R_A V_r + F_{Lf}A_L \quad (1)$$

$$N_{Gf}(1 - y_{Af}) = N_{Go}(1 - y_{Ao} - y_{Bo}) \quad (2)$$

- Material balance of liquid reactant

$$F_{Lf}(B_{Lf} - B_L) = \upsilon R_A V_r \quad (3)$$

- Reactor energy balance

$$F_{Lf}\rho_L c_{pL}(T_{Lf} - T) + N_{Gf}c_{pG}T_{Gf} - N_{Go}c_{pG}(1 - y_{Bo})T + [(-\Delta H_R) + (-\Delta H_S)]R_A V_r + (-\Delta H_S)F_{Lf}A_L + H_{ag} - N_{Go}y_{Bo}(-\Delta H_V) - US(T - T_c) = 0 \quad (4)$$

- Rate of gas absorption

$$N_A = a k_G V_r(p_{AG} - p_{Ai}) = a k_L V_r A_i E_A^* = (R_A V_r + F_{Lf}A_L) \quad (5)$$

Noteworthy and new characteristics of the model include the parameters H_{ag} and k_G. H_{ag} is a measure of heat addition due to agitation and sparging; whereas k_G is a measure of gas-side resistance to mass transfer which has been ignored in all previous models of bimolecular second-order reactions. Heat addition due to agitation and sparging is estimated here on the basis of the premise that the total mechanical power dissipated to the reaction mixture is converted into heat.

The description of interphase diffusion-reaction effects by the reaction (or enhancement) factor, E_A^*, in modeling gas–liquid reactors is essential for rational analysis of reactor performance. The reaction factor can be evaluated by coupling and solving the appropriate ordinary or partial differential equations (depending on whether the film or surface-renewal theory is used) with Eqs. (1)–(5). For non-linear kinetics, it is desirable to employ closed-form expressions for E_A^* to reduce complexity of the numerical computations. Past research has employed the approximate expression of Teramoto et al. [28] in the case of a non-volatile liquid reactant, and the expression of Shaikh–Varma [29] in the case of a volatile liquid. Derivation of both expressions is rooted in the rectangular simplification of the gas–liquid interfacial region. As the model we develop in the present investigation involves an explicit account of bubble size (see Table 1), it becomes prudent to account for bubble sphericity. Hence, the closed-form expression recently reported by Shaikh et al. [30] has been utilized in the reactor simulations presented in the next section. Although this expression is given by a set of non-linear simultaneous, transcendental, equations, it is still numerically advantageous compared to the relevant set of differential equations.

The reactor model equations can be recast in dimensionless form as shown below:

- Conversion of gaseous reactant

$$x_A = \frac{(\alpha + \beta)\theta + p' q a_L - \beta\theta_c - r(\theta_r - 1) + \nu y_B^* - H_p}{B' + (1 + \theta)r y_{Af} + \nu y_{Af} y_B^*} \quad (6)$$

- Conversion of liquid reactant

$$x_B = \nu\left[\left(\frac{Q}{q}\right)x_A - a_L\right] \quad (7)$$

- Temperature of reaction mixture

$$\theta = \frac{[B' + y_{Af}(r + \nu y_{Bo}^*)]x_A - p' q a_L + \beta\theta_c + r(\theta_r - 1) - \nu y_{Bo}^* + H_p}{(\alpha + \beta - r y_{Af} y_{Bo}^*)} \quad (8)$$

- Interfacial concentration of gaseous reactant

$$a_i = \frac{(1 - y_{Bo})(1 - x_A)H_o \exp[\delta/(1 + \theta)]}{(1 - y_{Af}x_A)\{1 + \exp[\delta/(1 + \theta)]\psi E_A^*\}} \quad (9)$$

Table 2
Reference values of key parameters used in numerical simulations

Parameter	Value
ρ_{Gf}	4.2×10^{-5} mol cm^{-3}
ρ_{Lf}	5.13×10^{-3} mol cm^{-3}
ρ_c	5.56×10^{-2} mol cm^{-3}
λ_c	7.139×10^{-4} cal s^{-1} cm^{-1} K^{-1}
A_{Gf}	4.2×10^{-5} mol cm^{-3}
B_{Lf}	5.1×10^{-3} mol cm^{-3}
H_o	0.00188
c_{pc}	18.0 cal mol^{-1} K^{-1}
D_T	30.5 cm
$(-\Delta H_R)$	26000 cal mol^{-1}
$(-\Delta H_S)$	4500 cal mol^{-1}
$(-\Delta H_V)$	9000 cal mol^{-1}
E	29000 cal mol^{-1}
T_{Lf}	297 K
T_{ci}	293 K
T_{co}	303 K
V_r	4000 cm^3
P	1.0 atm

- Reaction factor

$$E_A^* = M\sqrt{b_i}\left\{\frac{\Omega[M_1(1+\Omega)-1]+(1+\Omega)^2M\sqrt{b_i}\tanh[(1+(1/\Omega))M\sqrt{b_i}]}{\Omega[M_1(1+\Omega)-1]\tanh[(1+(1/\Omega))M\sqrt{b_i}]+(1+(1/\Omega))^2M\sqrt{b_i}}\right\}+\frac{1}{(1+\Omega)}$$
$$-\frac{\Omega(1+\Omega)\beta' a_0}{\Omega[M_1(1+\Omega)-1]\sinh[(1+(1/\Omega))M\sqrt{b_i}]+(1+\Omega)^2M\sqrt{b_i}\cosh[(1+(1/\Omega))M\sqrt{b_i}]} \quad (10)$$

where

$$b_i = \frac{(1+rq)-E_A^*-a_L}{rq} \quad (11)$$

$$a_L = \frac{\Omega(1+\Omega)M\sqrt{b_i}+\Omega^2\beta' a_0\sinh[(1+1/\Omega)M\sqrt{b_i}]}{\Omega[M_1(1+\Omega)-1]\sinh[(1+1/\Omega)M]+(1+\Omega)^2M\sqrt{b_i}\cosh[(1+1/\Omega)M\sqrt{b_i}]} \quad (12)$$

$$M_1 = M^2[[\Omega/(1+\Omega)]\alpha' - [1+(1/\Omega)+(1/3\Omega^2)]+[\Omega/(1+\Omega)]\beta' \quad (13)$$

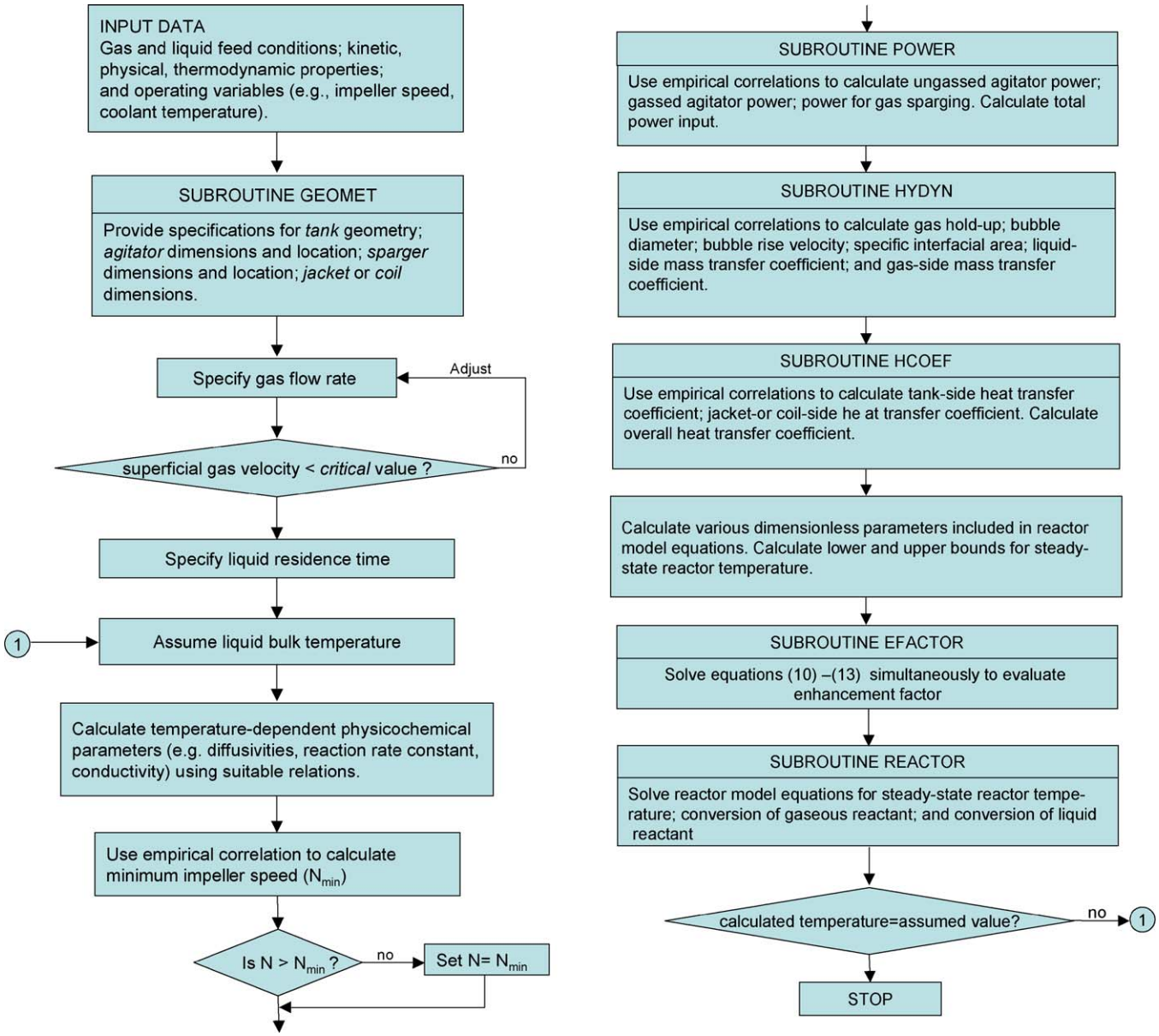

Fig. 2. Flowchart for numerical solution of reactor model equations.

3.2. Transport, hydrodynamic, and allied parameters

Close examination of the preceding equations shows that the reactor model can be solved once the values of several parameters are specified. Further examination shows that the parameter values depend on specification of basically four groups of parameters: (a) physical, chemical, and thermodynamic properties of the reacting reagents; (b) operating variables, such as flow rates, concentration and temperature of the each feed stream, and impeller speed; (c) transport parameters; (d) hydrodynamic parameters. Group (c) includes mass and heat transfer coefficients: k_G, k_L, and U. Group (d) includes: interfacial area a, gas holdup ε_G, bubble diameter d_b, and total power input due to agitation and aeration, P_T. The computation of group (c) and group (d) parameters in turn depends on what may be termed allied parameters; namely: tank-side (h_T) and jacket- or coil-side heat transfer coefficients (h_j or h_c); bubble terminal rise velocity; minimum impeller speed; and power inputs due to agitation and aeration. Many correlations for predicting transport, hydrodynamic, and allied parameters in agitated reactors have been proposed in the literature. The correlations that we apply here are given in Table 1. These were selected from an extensive review of the relevant literature that included numerous correlations for most of the parameters listed. Analysis of these correlations is beyond the scope of the present study. Suffice it to say here that the selection process involved range of applicability and accuracy of the correlation, nature of reacting species, and vessel and impeller geometry, among other factors.

4. Results and discussion

In contrast to other models in the literature, the model presented in the previous section enables us to investigate the influence of several important elements on multiplicity in agitated gas–liquid reactors. To carry out detailed investigations using Eqs. (6)–(13), specifications of a standard-configuration reactor (as given in Fig. 1), and the correlations given in Table 1, necessitated the development of a generalized, flexible, numerical code. For the sake of brevity, details of the code are not provided here, however the strategy of the numerical solution is outlined in Fig. 2. All previous simulation studies of second-order bimolecular reactions in gas–liquid agitated reactors were performed using constant values of physical and thermodynamic properties, transport, and hydrodynamic parameters. In most cases these values were selected to be identical to those for the chlorine–*n*-decane system [1]. Although reaction kinetics of this system are more complex than the second-order case, it has been gainfully employed as representative of exothermic gas–liquid reactions. Therefore, we have selected this system for our numerical simulations in order: to test the applicability of the new model; to compare our results with those of previous investigations in regard to the existence of bifurcations; and to analyze effect of the new parameters introduced in the present model. Nevertheless, we should emphasize that the variation of transport and hydrodynamic parameters is explicit in our model, and that the variation of temperature-sensitive physical, and chemical properties of the system (namely, diffusivity, heat capacity, viscosity, surface tension, and thermal conductivity) has also been accounted for. Table 2 lists values of the parameters used in the reactor simulations presented next, except where otherwise noted.

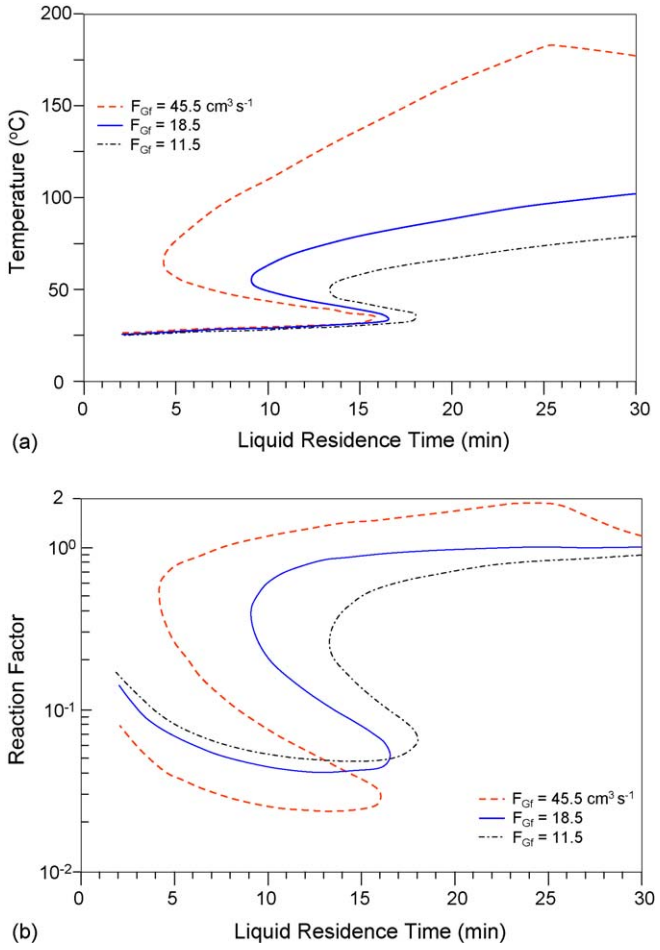

Fig. 3. (a) Effect of gas and liquid flow rates on steady state temperature (k [50 °C] = 5.0 cm^3 mol^{-1} s^{-1}; N = 15 rps; θ_r = 1; y_{Af} = 0.7; y_{Bo} = 0). (b) Effect of gas and liquid flow rates on reaction factor (k [50 °C] = 5.0 cm^3 mol^{-1} s^{-1}; N = 15 rps; θ_r = 1; y_{Af} = 0.7; y_{Bo} = 0).

4.1. Effect of gas and liquid residence times

The transport and hydrodynamic parameters are strongly dependent on the superficial gas velocity. Fig. 3(a) presents an example of an S-shaped multiplicity pattern, showing the effect of gas and liquid flow rates on reactor temperature. We observe that the upper temperature branch is more sensitive to gas flow rate, because in that region the reaction rate increases with the increase in gas flow rate as shown in Fig. 3(b). In Fig. 3(a), we also note that the steady state temperature corresponding to F_{Gf} = 45.5 cm^3 s^{-1} reaches a maximum and starts decreasing sharply with further increase in the liquid residence time. At this point the conversion of liquid reactant is almost complete and the liquid reactant is exhausted; as a result the rate of reaction decreases and so does the steady state temperature. Fig. 3(b) also shows that on the low branch, the reaction factor decreases with the increase in gas flow rate. This indicates that at high gas

flow rates and low temperature conditions the rate of absorption of gaseous reactant is very high compared to its consumption in the liquid film. As a result all the gaseous reactant goes into the liquid bulk. It is clear then that corresponding to the upper temperature branch, the increase in gas flow rate causes a sharp increase in the rate of reaction due to the change in physico-chemical, hydrodynamic and transport parameters.

Fig. 4(a) shows the effect of change in gas and liquid flow rates on the power input to the reactor. It can be seen that an increase in the gas flow rate increases the total specific power

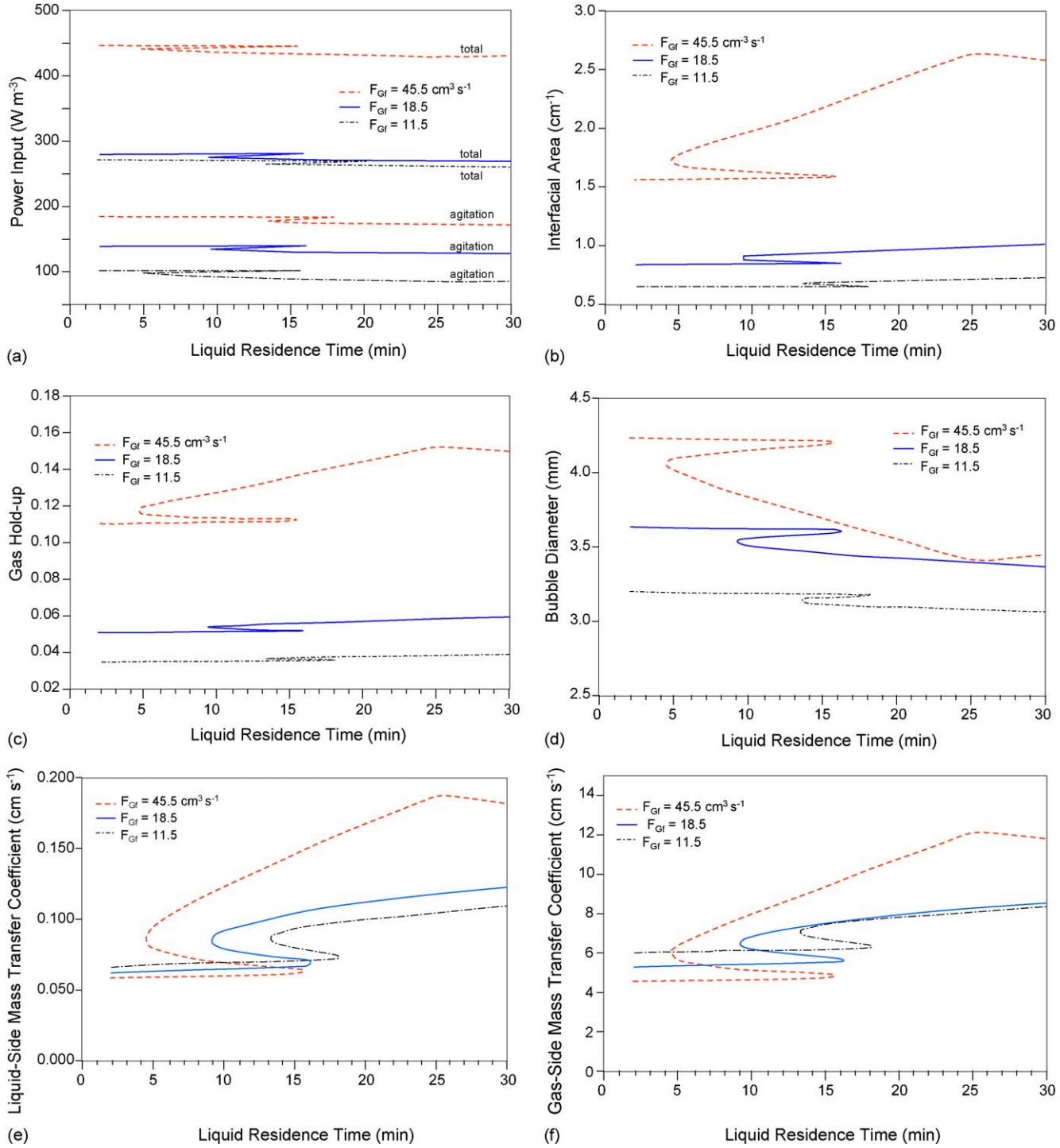

Fig. 4. (a) Effect of gas and liquid flow rates on power input (k [50 °C] = 5.0 cm^3 mol^{-1} s^{-1}; N = 15 rps; θ_r = 1; y_{Af} = 0.7; y_{Bo} = 0). (b) Effect of gas and liquid flow rates on interfacial area (k [50 °C] = 5.0 cm^3 mol^{-1} s^{-1}; N = 15 rps; θ_r = 1; y_{Af} = 0.7; y_{Bo} = 0). (c) Effect of gas and liquid flow rates on gas hold-up (k [50 °C] = 5.0 cm^3 mol^{-1} s^{-1}; N = 15 rps; θ_r = 1; y_{Af} = 0.7; y_{Bo} = 0). (d) Effect of gas and liquid flow rates on mean bubble diameter (k [50 °C] = 5.0 cm^3 mol^{-1} s^{-1}; N = 15 rps; θ_r = 1; y_{Af} = 0.7; y_{Bo} = 0). (e) Effect of gas and liquid flow rates on liquid-side mass transfer coefficient (k [50 °C] = 5.0 cm^3 mol^{-1} s^{-1}; N = 15 rps; θ_r = 1; y_{Af} = 0.7; y_{Bo} = 0). (f) Effect of gas and liquid flow rates on specific gas-side mass transfer coefficient (k [50 °C] = 5.0 cm^3 mol^{-1} s^{-1}; N = 15 rps; θ_r = 1; y_{Af} = 0.7; y_{Bo} = 0). Specific gas-side mass transfer coefficient is $k_G RT_{Gf}$.

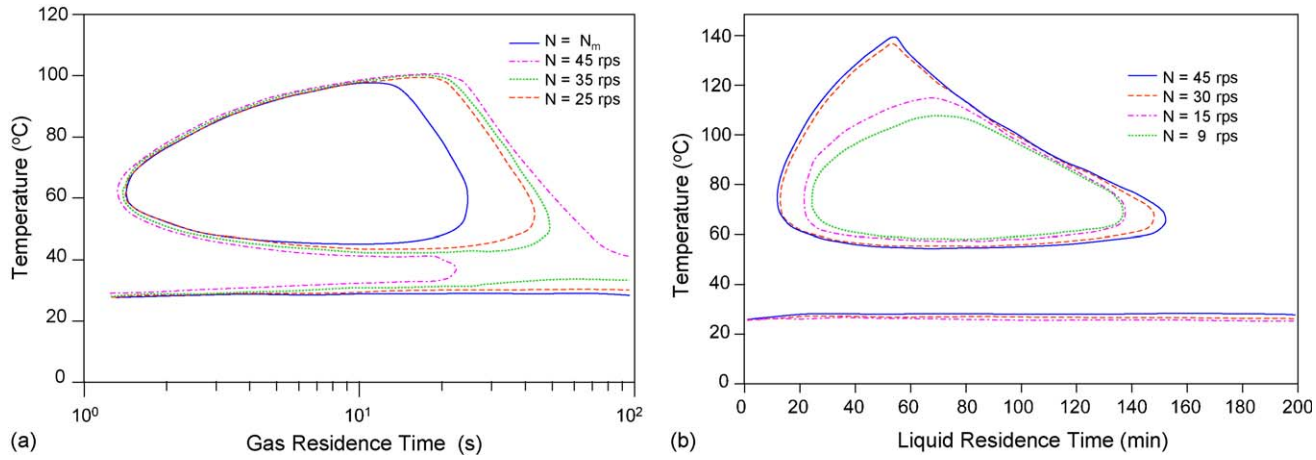

Fig. 5. (a) Effect of impeller speed and gas residence time on steady state temperature (k [50 °C] = 3.0 cm^3 mol^{-1} s^{-1}; θ_r = 1; y_{Af} = 0.5; y_{Bo} = 0; τ_L = 600 s). (b) Effect of impeller speed and liquid residence time on steady state temperature (k [50 °C] = 0.9 cm^3 mol^{-1} s^{-1}; F_{Gf} = 18.5 cm^3 s^{-1}; θ_r = 1; y_{Af} = 0.7; y_{Bo} = 0).

input and decreases the power input due to agitation, as the presence of gas reduces the drag coefficient of the impeller blade by forming gas cavities at the rear of each blade. It is also seen that the reduction in power drawn by the impeller is higher at higher gas flow rates. At higher gas flow rates the size of the gas cavities is larger and thus the drag coefficient is smaller. The middle and lower branches in each curve of Fig. 4(a) demonstrate the effect of change in physicochemical properties, mainly the viscosity in this case, due to the change in temperature. Fig. 4(b) and (c) show that an increase in the gas flow rate increases the specific interfacial area and gas hold-up; indeed a three-fold increase is possible. This is due to the increase in superficial gas velocity and total specific power input. Fig. 4(d) shows that the mean bubble diameter also increases with the increase in gas flow rate despite the fact that the total specific power input is increased, indicating that under present conditions the effect of superficial gas velocity, to which the bubble diameter is directly proportional, is dominating. Fig. 4(e) shows that the gas flow rate has no significant influence on the liquid-side mass transfer coefficient k_L. However, k_L rapidly increases with the increase in temperature, because both diffusivity and viscosity are greatly affected by the change in temperature. On the other hand, Fig. 4(f) reveals that the gas-side mass transfer coefficient k_G decreases with the increase in gas flow rate, since at higher gas flow rates, relatively larger-sized bubbles are formed, as shown in Fig. 4(d). At higher temperature the value of k_G is higher due to smaller bubble size and higher gas diffusivity.

4.2. Effect of impeller speed

Fig. 5(a) and (b) show the effect of impeller speed on steady-state multiplicity. Fig. 5(a) shows that the region of multiplicity expands with the increase in impeller speed towards higher gas residence times. We also note that the increase in impeller speed has no effect on the multiplicity in case of relatively higher gas flow rates, i.e. lower gas residence times. This can be explained as follows. First, at higher gas residence times, an increase in impeller speed increases the value of parameter H_{ag} in Eq. (4), indicating that under such conditions the contribution of heat dissipated by agitation becomes significant in the overall heat buildup of the system. Secondly, at low gas flow rates, the interfacial area, gas hold-up and mass transfer coefficients are much higher at high impeller speeds. Therefore, a change in the degree of agitation may change the regions and patterns of multiplicity

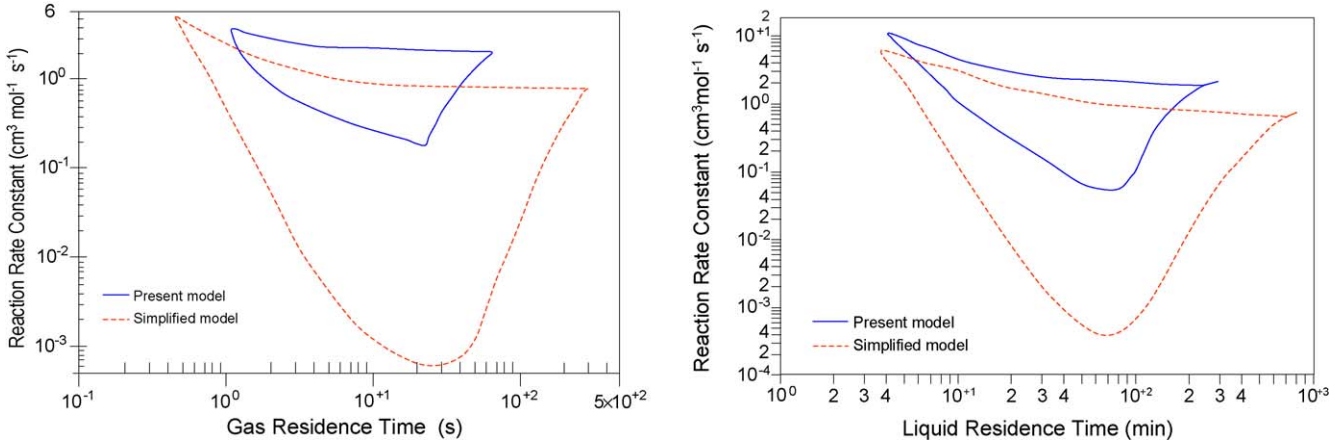

Fig. 6. (a) Model comparison of uniqueness and multiplicity regions; multiplicity within enclosed areas (variable N; θ_r = 1; y_{Af} = 0.7; y_{Bo} = 0; τ_L = 600 s). (b) Model comparison of uniqueness and multiplicity regions; multiplicity within enclosed areas (N = 15 rps; F_{Gf} = 18.5 cm^3 s^{-1}; θ_r = 1; y_{Af} = 0.9; y_{Bo} = 0).

(e.g. from isola to S-shaped) due to the change in rate of reaction caused by the combined effect of the above factors. Fig. 5(b) shows the effect of impeller speed on reactor temperature with variation in liquid residence time. Here again we note that the effect of impeller speed is more pronounced in the region of low F_{Gf}/F_{Lf} ratios due to the same reasons discussed above. We further note that there exists a maximum impeller speed beyond which the multiplicity region is not affected by the impeller speed.

4.3. Comparison of reactor models

Fig. 6(a) and (b) present a comparison of the multiplicity regions predicted by the model developed in this work and the relatively simplified model reported in [13]. We observe that the multiplicity region in the reactivity-residence time parameter space, predicted by the present model, is much smaller compared to that predicted by the simpler model. A comparison of various multiplicity patterns predicted by the new and simplified models also has been carried out. The new model predicts all three types of multiplicity patterns (S-type, mushroom-type, and isola-type) reported before, however, in all cases the regions and the patterns of multiplicity predicted by new model are remarkably different from those predicted by the old model. We also note that in all the cases presented here, the upper temperature branch predicted by new model is always lower than that predicted by simplified model. This large difference in predictions of the two models is due to the fact that possible variations of hydrodynamic and transport parameters with operating conditions are accounted for as opposed to the uniform values used in the simulation based on the simplified model.

5. Concluding remarks

A generalized model for the steady-state performance of non-isothermal gas–liquid mechanically agitated reactors has been presented in this work. The unique feature of the model is that it combines, for the first time, the complex interactions involved in the modeling of this reactor, i.e. reaction kinetics, interphase mass transfer, physical contacting, and reactor and impeller geometry. The model incorporates empirical correlations and data for key parameters which have been selected from an extensive review of the literature on transport, hydrodynamic, and allied parameters. It appears that the only other agitated gas–liquid reactor modeling study in which such an explicit accounting of hydrodynamic and transport parameters was done is that reported in [41], however, that study only addressed isothermal reactor performance.

An extensive parametric-sensitivity analysis has been carried out wherein the predictions of the new reactor model have been compared with those of earlier simplified models. The results show that regions in different parameter spaces in which multiplicity exists are considerably reduced with application of the generalized model. Although the new model predicts the same multiplicity patterns and maximum number of multiple steady states, the conditions under which they occur can be markedly different for the two models. Moreover, in certain cases the new model predicts uniqueness while the simplified model predicts multiplicity or vice versa.

The signal effect of the degree of agitation on non-isothermal reactor behavior is analyzed here apparently for the first time. It is interesting to observe that the impeller speed can be an important factor in the existence of steady-state multiplicity. The simulation results show that this effect is more important in the case of variation in gas residence time. Our findings indicate that simulation based on the new model is more realistic, as our simulations demonstrate that hydrodynamic, transport, and allied parameters are more sensitive to changes in the gas residence time compared to changes in the liquid residence time. It appears that previous studies probably overpredicted the regions of multiplicity. Therefore, earlier results on steady state multiplicity in agitated gas–liquid reactors with bimolecular reactions can be considered conservative.

Acknowledgment

The authors are grateful to King Fahd University of Petroleum & Minerals for support of this work.

References

[1] J.S.Y. Ding, S. Sharma, D. Luss, Ind. Eng. Chem. Fund. 13 (1974) 76.
[2] S. Raghuram, Y.T. Shah, Chem. Eng. J. 13 (1977) 81.
[3] S. Raghuram, Y.T. Shah, J.W. Tierney, Chem. Eng. J. 17 (1979) 63.
[4] D.T.J. Huang, A. Varma, Chem. Eng. J. 21 (1981) 47.
[5] D.T.J. Huang, A. Varma, AIChE J. 27 (1981) 481.
[6] D.T.J. Huang, A. Varma, AIChE J. 27 (1981) 489.
[7] C.P.P. Singh, Y.T. Shah, N.L. Carr, Chem. Eng. J. 23 (1982) 101.
[8] A.A. Shaikh, A. Varma, Chem. Eng. J. 29 (1984) 59.
[9] A.A. Shaikh, A. Varma, Am. Chem. Soc. Symp. Ser. 237 (1984) 79.
[10] K.R. Westerterp, P.R.J.J. Crombeen, Chem. Eng. Sci. 38 (1983) 1331.
[11] D. White, L.E. Johns, AIChE J. 32 (1986) 981.
[12] A.A. Shaikh, Chem. Eng. Commun. 52 (1987) 331.
[13] A.A. Shaikh, S. Batran, S.M. Zarook, Proceedings of the Third Saudi Engineering Conference, King Saud University, Riyadh, 1991, p. 372.
[14] E.F. Stefaglo, A.V. Kuchin, A.V. Kravstov, Chem. Eng. Sci. 59 (2004) 4137.
[15] F. Kastanek, J. Zahradnik, J. Kratochvil, J. Cermak, Chemical Reactors for Gas–Liquid Systems, Ellis-Horwood, Chichester, 1993.
[16] R. Mann, Gas–Liquid Contacting in Mixing Vessels, The Institution of Chemical Engineers, England, 1983.
[17] K. Schugerl, A. Lubbert, T. Korte, J. Diekmann, Int. Chem. Eng. 27 (1987) 583.
[18] D. Ridgway, R.N. Sharma, T.R. Hanley, Chem. Eng. Sci. 44 (1989) 2935.
[19] J.B. Joshi, T.A. Patil, V.V. Ranade, Y.T. Shah, Rev. Chem. Eng. 6 (1990) 76.
[20] N. Harnaby, M.F. Edwards, Mixing in the Process Industries, Butterworths, London, 1985.
[21] A. Steiff, R. Poggermann, P.M. Weinspach, Ger. Chem. Eng. 4 (1981) 30.
[22] D.S. Dickey, Chem. Eng. Prog. (1991) 22.
[23] A.W. Niewnow, D.J. Wisdom, Chem. Eng. Sci. 29 (1974) 1994.
[24] R.V. Calabrese, C.M. Stoots, Chem. Eng. Prog. (1989) 43.
[25] A.W. Niewnow, D.J. Wisdom, J.C. Middleton, Proceedings of the Second European Conference on Mixing, BHRA Fluid Engineering, Cranfield, 1977.
[26] R. Mann, Chem. Eng. Res. Des. 64 (1986) 23.
[27] A.W. Niewnow, Chem. Eng. Prog. (1990) 61.

[28] M. Teramoto, T. Nagayasu, K. Matsui, K. Hashimoto, S. Nagata, J. Chem. Eng. 2 (1969) 186.
[29] A.A. Shaikh, A. Varma, Chem. Eng. Sci. 39 (1984) 1639.
[30] A.A. Shaikh, A. Jamal, S.M. Zarook, Chem. Eng. J. 57 (1995) 27.
[31] B.D. Prasher, G.B. Wills, Ind. Eng. Chem. Proc. Des. Dev. 12 (1973) 351.
[32] M.M. Sharma, R.A. Mashelkar, Inst. Chem. Eng. Symp. Ser. 28 (1968) 10.
[33] P. Kurpiers, A. Steiff, P.M. Weinspach, Ger. Chem. Eng. 8 (1985) 48.
[34] K.B. Rao, P.S. Murthy, Ind. Eng. Chem. Proc. Des. Dev. 12 (1973) 190.
[35] I.H. Lehrer, Ind. Eng. Chem. Proc. Des. Dev. 9 (1970) 553.
[36] F. Bondy, S. Lippa, Chem. Eng. (1983) 62.
[37] D.N. Miller, AIChE J. 20 (1974) 445.
[38] M.E. Abu El-Hassan, Chem. Eng. Commun. 22 (1983) 243.
[39] M.M.C.G. Warmoeskerken, J.M. Smith, Chem. Eng. Sci. 40 (1985) 2063.
[40] P.H. Calderbank, M.B. Moo-Young, Trans. Inst. Chem. Eng. 39 (1961) 337.
[41] J. Markos, M. Pisu, M. Morbidelli, Comput. Chem. Eng. 22 (1998) 627.